THE ASTROPHYSICAL JOURNAL, 302:809–825, 1986 March 15

THE DYNAMICS OF MAGNETICALLY TRAPPED FLUIDS. I. IMPLICATIONS FOR UMBRAL DOTS AND PENUMBRAL GRAINS[1]

ARNAB RAI CHOUDHURI[2]
Enrico Fermi Institute and Department of Physics, University of Chicago
Received 1985 June 3; accepted 1985 September 13

ABSTRACT

We present a study of the magnetohydrodynamic system in which a nonmagnetized fluid in a gravitational field is surrounded by a fluid carrying a vertical magnetic field. It is pointed out that this study can throw some light on the fine-structural features of a sunspot. The equilibrium configuration of the field-free fluid is a tapering column ending at an apex. The regions away from the apex can be studied by the *slender flux tube approximation.* A scheme developed to treat the apex indicates that, just below the apex, the radius of the tapering column opens up with a 3/2 power dependence on the depth below the apex. If the internal pressure of the field-free fluid is increased, the apex rises, and a static equilibrium may not be possible beyond a limit if the magnetic pressure drops quickly above a certain height. The nature of steady-flow solutions beyond this limit is investigated. Under conditions inside a sunspot, a column of field-free gas is found to rise with a velocity of about 100 km hr^{-1}. If umbral dots and penumbral grains are interpreted as regions where the field-free gas ultimately emerges, we get a very natural explanation of most of their observed properties.

Subject headings: hydromagnetics — Sun: magnetic fields — Sun: sunspots

I. INTRODUCTION

The study of magnetic flux tubes, which are regions of high magnetic field surrounded by field-free fluids, has been a classical research topic of magnetohydrodynamics for a long time (Parker 1979*a*; Priest 1982). However, almost no attention has been paid to a system which is, in a sense, complementary to a flux tube: a column of field-free fluid surrounded by regions of high magnetic field. The aim of the present investigation is to understand the basic physics of such a system. Since the net magnetic flux through any cross section of a flux tube is an invariant for the tube, the tube cannot terminate at a point in space (at least in a commonplace world without magnetic monopoles!) However, our field-free fluid column does not have any analogous invariant and hence can begin or end under suitable circumstances. Consequently the behavior of such a system is quite different from that of a flux tube.

The study of such field-free fluid columns is not just a mathematical exercise. We shall see that our study helps us to understand some of the fine-structural features of a sunspot. Recent theoretical and observational works tend to support the view that a sunspot is a collection of fibril flux tubes herded together rather than a homogeneous uniform object. It is well known that the magnetic field in the solar photosphere exists in the form of intense fibril flux tubes (Sheeley 1967; Livingston and Harvey 1969; Howard and Stenflo 1972; Frazier and Stenflo 1972; Stenflo; 1973; Chapman 1974). A sunspot is formed when a number of such tubes collect together as the result of processes which we still do not understand very well (Meyer *et al.* 1974; Parker 1979*b*). The intriguing question is whether these flux tubes retain their individual identities even after forming the sunspot, or whether they coalesce to form a monolithic single flux tube (Severny 1965; Gokhale and Zwaan 1972).

Magnetic fields embedded in electrically conducting fluids are well known to make the system more stable against convective instability (Thomson 1951; Chandrasekhar 1952, 1961, pp. 160–186; Gough and Taylor 1966; Proctor and Weiss 1982). Biermann (1941) explained the darkness of sunspots by suggesting that the magnetic field of the spot inhibits convection, thereby blocking the passage of heat from the interior to the solar surface. However, if such a large structure as a sunspot uniformly blocked convection everywhere throughout its volume, then large quantities of heat would pile up at the bottom and would disrupt the sunspot (Parker 1974*a*). In addition, unless the sunspot structure is very deep, the blocked heat would appear in a bright ring around the sunspot, which is not observed (Spruit 1977). A two-component model of sunspots was first suggested by Makita (1963) and later reemphasized by Obridko (1968*a b*; Mogilevsky *et al.* 1968) to explain the spectral lines of certain elements present in two states of ionization in the sunspot. Parker (1979*b*) showed that we can understand a number of otherwise puzzling properties of sunspots if we visualize them as collections of fibril flux tubes loosely clustered together, with convecting field-free fluid filling up the gaps between the tubes. In this "spaghetti model" we can avoid the difficulty of heat piling up below the sunspot, and we have a natural explanation of umbral bright dots (Obridko 1975; Parker 1979*b*, *c*). These dots are bright spots seen in the umbra and can be regarded as occasional upward intrusions of field-free fluid to the visible surface between the flux tubes.

Umbral bright dots were first observed by Chevalier (1916). The penumbra of a sunspot is also seen to possess elongated bright grains. The observational and theoretical aspects of the fine structures in sunspots have been reviewed respectively by Moore (1981) and Thomas (1981). Here we briefly summarize the highlights of observational results that we shall need for our discussion. Although there have been some stratospheric observations of sunspots (Danielson 1964; Krat, Karpinsky, and Pravdjuk 1972), most of the knowledge of sunspot fine structure comes from ground-based observations. Even the largest umbral dots seem to be

[1] Submitted to the Department of Physics, University of Chicago, in partial fulfillment of the requirements for the Ph.D. degree.
[2] Present address: High Altitude Observatory, National Center for Atmospheric Research.

beyond the resolution of ground-based observations, so that we have no direct information about their shapes and sizes. However, from measurements of the color index, Beckers and Schröter (1968; see also Koutchmy and Adjabshirzadeh 1981) concluded that the dots are of photospheric intensity with diameters of 150–200 km. The average lifetime of individual dots is about $\frac{1}{2}$ hr (Danielson 1964; Beckers and Schröter 1968; Adjabshirzadeh and Koutchmy 1980), although some of them have been seen to live longer than $2\frac{1}{2}$ hr (Bray and Loughhead 1964, pp. 87–88). This is much longer than the typical lifetime of photospheric granules ($\sim$10 minutes). Loughhead, Bray, and Tappere (1979) found umbral dots even in the darkest regions of large spots, although some previous observations failed to find dots in the innermost parts of the umbra (Beckers and Schröter 1968). Spectscopic observations indicate that the dots probably have much weaker magnetic fields than the surrounding umbra (Zwaan 1968; Zwaan and Buurman 1971; Kneer 1973) and are sites of upward fluid motion (Beckers and Schröter 1969; Kneer 1973). Kneer (1973) reported upward velocities as high as 3 km s^{-1}. However, one should take these results with some amount of caution, since they were obtained at the limit of resolution. It seems that we have to wait for the Solar Optical Telescope to go up before we can have really conclusive information on various properties of umbral dots.

Penumbral grains look like bright filaments elongated in the radial direction with respect to the center of the sunspot and separated from each other by dark lanes. Their properties have been studied by Muller (1973*a*, *b*, 1976, 1981) from a series of high-quality photographs taken at Pic du Midi. The grains seem to have an average brightness slightly less than the photospheric brightness and an average width of about 270 km, with lengths equal to a few times the widths (Muller 1973*b*; Bonet, Ponz and Vazquez 1982). The lifetime was found to be of the order of 1 hr, although it depended on the position inside the penumbra (Muller 1973*a*). Muller also made the striking observation that the grains move toward the umbra with a velocity approaching 0.5 km s^{-1}, and if they live long enough to enter the umbra, then they start looking like umbral dots (Muller 1973*a*, 1976; Tönjes and Wöhl 1982; Soltau 1982). Beckers and Schröter (1969) found that the bright grains in the penumbra move upward with respect to the dark regions, and there is evidence that they have weaker magnetic fields than the dark regions (Beckers and Schröter 1969; Abdussamatov 1976). Thus umbral dots and penumbral grains both seem to be regions of photospheric brightness, weaker magnetic field, upwelling fluid motion, and comparble lifetimes. The main difference between them is the elongated shape of the grains, although grain widths seem to be comparable to dot diameters. It has been suggested that umbral dots and penumbral grains are probably manifestations of the same physical processes (Moore 1981; Moore and Rabin 1985).

Since umbral dots and penumbral grains in low-resolution photographs resemble photospheric granules, it was suggested that the sunspot magnetic field does not inhibit convection completely, and the dots and grains are just convective cells within the sunspot (Bumba, Hejna, and Suda 1975; Hejna 1977; Bumba and Suda 1980). However, Loughhead, Bray, and Tappere (1979) point out that this apparent resemblance disappears as the resolution is improved (see also Adjabshirzadeh and Koutchmy 1982; Lawrence 1983). Dot diameters and grain widths are much smaller than photospheric granule sizes, and their lifetimes are considerably longer than those of the granules. Beckers and Schröter (1968) further point out that umbral dots "do not form a kind of closed pattern as observed in the photosphere. They appear rather as isolated emission points." However, it has recently been argued by Knobloch and Weiss (1984) that a magnetoconvective theory of the origin of umbral dots may be made to work by going into sufficiently nonlinear regimes. Although the rather sketchy suggestions of Knobloch and Weiss (1984) seem interesting, a more extensive analysis to substantiate those suggestions has not yet been carried out. Wilson (1969, 1972) made another suggestion that the umbral dots are shallow regions where Alfvén waves traveling through sunspots dissipate energy due to high field gradients. Apart from the fact that this suggestion begs the question of what created the field gradients, it seems unlikely on the basis that later observations failed to detect the existence of Alfvén waves above sunspots (Beckers and Schneeberger 1977).

Parker's idea (1979*b*, *c*) that an umbral dot is an intrusion of field-free fluid through the flux tubes seems to be the most satisfactory idea to this date. Parker (1979*c*) calculated the overstable modes for a vertical slab of field-free fluid sandwiched between regions of vertical magnetic field. He found that, if the field-free fluid is convectively unstable, then there can be vertical oscillations of period 10^2 s with a growth time of 1–3 hr. Since this growth time is comparable to the lifetime of dots, it was suggested that the dots represent the nonlinear growth of these oscillations punching through to the visible surface. However, we expect the magnetic field to close on the field-free fluid from the top and to control the dynamic behavior of the system. Parker did not consider this aspect of the problem, which the present paper aims to study. We shall see that, from a consideration of these aspects, we can have a more natural explanation of the upward flow in umbral dots.

We discuss in § II the static configuration of a field-free fluid column trapped by magnetic fields and show that it takes up a tapering shape as shown in Figure 1*a*. Sections III and IV demonstrate, for an incompressible fluid and for a polytropic atmosphere, respectively, that the field-free fluid column rises if the internal pressure of the field-free fluid is increased. In the photosphere the magnetic field of a sunspot is contained by the surrounding gas pressure, and, if we go sufficiently deep in the sunspot, the field can be regarded as vertical. However, higher in the photosphere, the gas pressure drops considerably. Consequently, the magnetic field

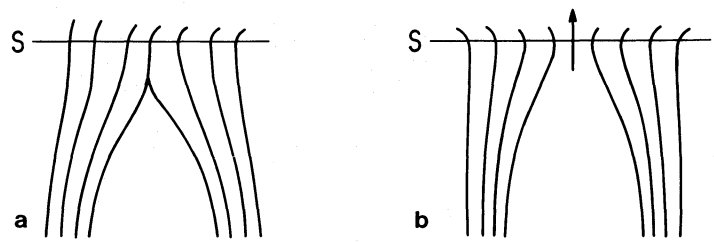

FIG. 1.—Field-free fluid surrounded by the magnetized fluid with magnetic pressure dropping above the surface *S*. (*a*) The apex has not yet reached the surface *S*. (*b*) A flow path has been established.

bulges out, making the magnetic pressure fall. To facilitate our calculations, we make a simplifying assumption that the magnetic field is constrained to remain vertical up to a certain height S, and then the field pressure suddenly becomes negligible above that height. As the pressure of the field-free fluid is increased, the apex of the column rises higher and higher, until it reaches the surface S, and ultimately the trapped fluid is expected to burst forth as shown in Figure 1*b*. Steady-flow solutions of this kind are considered in §§ III and IV.

This is probably what happens in reality with the umbral dots in a sunspot. Convection takes place in the trapped field-free fluid, whereas the magnetic field around it makes those regions stable against convection. Hence heat can be transported convectively upward into the trapped fluid, but no further convective transport is possible to allow that heat to reach the surface. We thus expect to have a situation where the temperature and pressure of the trapped fluid keep growing, unless radiative diffusion is effective. A discussion of radiative diffusion under conditions of the solar convective zone is presented in § V and suggests that the apex of a field-free column may indeed rise, allowing more field-free fluid to squeeze in between the magnetic field lines. Ultimately a flow path is forced through to the surface. However, after a sufficient amount of field-free fluid has escaped, thereby reducing its internal pressure, it may no longer be possible to maintain a flow path and the field may again close up, stopping the escape of the field-free fluid. Thus the field geometry effectively acts as a *magnetic valve*. When there is sufficient pressure under it, the *magnetic valve* opens and allows the trapped fluid to come out. But after enough fluid has escaped to reduce the pressure sufficiently, the *magnetic valve* closes and chokes off the flow. An umbral dot can be regarded simply as an open *magnetic valve* through which field-free gas from below is coming out. Section V takes up the question: How well can we understand the observed properties of umbral dots and penumbral grains from such ideas?

In order to pose a consistent mathematical problem, we need a boundary condition away from the field-free fluid column. In the present preliminary investigation, we use the condition that the magnetic field lines become vertical at some distance away from the field-free column, implying that the effect of the column's presence ceases to be felt beyond that distance. This assumption, as well as the other assumption of pressure dropping off above a surface S, are probably not too unrealistic in the solar context. Still, the ultimate justification for what we are doing lies in the fact that the simplifications introduced here make an otherwise impossible problem tractable.

II. STATIC EQUILIBRIUM

We assume our fluids to be perfect conductors of electricity so that the field-free fluid and the magnetized fluid remain two distinct entities. In this section and the next, we mainly consider the fluids to be incompressible. We first find the static equilibrium solution where the field-free fluid takes the shape of a tapering column surrounded by the magnetized fluid. The boundary condition to be satisfied across the surface of separation is

$$p_i = p_e + \frac{B^2}{8\pi}, \tag{1}$$

where p_i and p_e are the internal and external fluid pressures, and B is the amplitude of the magnetic field just outside the boundary. Thus we are faced with one of those notorious problems where, though the boundary condition is known, the boundary is not specified in advance but has to come as a part of the solution. We now discuss how this problem can be tackled in two and three dimensions.

a) Two-dimensional Case

Let us take the x-axis in the vertical direction (x increasing downward) and the y-axis in the horizontal direction. Let

$$y = \pm y_s(x)$$

be the boundary separating the two fluids, $y = 0$ being the central axis of the field-free column. We have a reasonable estimate of $y_s(x)$ if we make two assumptions. The first assumption is that at a distance $y = Y$ the magnetic field becomes vertical. Hence a fixed amount of flux (which we call $B_0\, Y$) is confined between $y = y_s(x)$ and $y = Y$. The second assumption is the *slender flux tube approximation* (Roberts and Webb 1978; Parker 1979*a*, pp. 123–127; Priest 1982, pp 314–318), which has proved particularly helpful in a large number of flux-tube problems (Parker 1974*b*; Defouw 1976; Roberts and Webb 1978; Webb and Roberts 1978; Spruit 1979; Spruit and Zweibel 1979; Hasan 1984). In this approximation, the variations of different physical quantities across a transverse cross section are neglected. In our case we assume that the various physical quantities do not change over a transverse section of the tapering column of field-free fluid, and the same is assumed true for the surrounding fluid. One straightforward implication of this approximation is that the magnetic field at a particular height x is given by

$$B(x)[Y - y_s(x)] = B_0\, Y\,. \tag{2}$$

The internal and external pressures for incompressible fluids can be written as

$$p_i = \rho_i g x + c_i\,, \qquad p_e = \rho_e g x + c_e\,, \tag{3}$$

in terms of the uniform densities ρ_i and ρ_e, where c_i and c_e are constants. From equations (1)–(3) we obtain

$$(\rho_i - \rho_e) g x + (c_i - c_e) = \frac{B_0^2}{8\pi}\left[1 - \frac{y_s(x)}{Y}\right]^{-2}. \tag{4}$$

If $x = x_0$ is the tip of the column where $y_s(x)$ goes to zero, then

$$c_i - c_e = \frac{B_0^2}{8\pi} - (\rho_i - \rho_e) g x_0\,,$$

so that equation (4) becomes

$$\frac{y_s(x > x_0)}{Y} = 1 - \left[1 + \frac{8\pi\Delta\rho g Y}{B_0^2}\left(\frac{x}{Y} - \frac{x_0}{Y}\right)\right]^{-1/2}, \tag{5}$$

where $\Delta\rho = \rho_i - \rho_e$. This equation gives $y_s(x)/Y$ as a function of x/Y when $\Delta\rho g Y/B_0^2$ is specified.

The solid curve in Figure 2 shows $y_s(x)/Y$ for $\Delta\rho g Y/B_0^2 = 0.118$, whereas the dotted curve is the result of a numerical calculation without using the slender flux tube approximation. In our numerical calculation, we assumed that the field overpowers the magnetized fluid and can be treated as a potential field. Hence we solved for a potential field in the magnetized fluid with the boundary conditions that it becomes vertical at $y = Y$ and the boundary $y_s(x)$ is so situated as to satisfy equation (1) along it. The filed lines of our numerical solution are shown in Figure 3. Comparing the solid and the dotted curves in Figure 2, we find that the slender flux tube approximation gives good results everywhere except near the apex. The numerical solution further shows that the value of the magnetic field across the tube at a horizontal level does not change by more than 20%, provided that we are not too near the apex. This justifies the use of the slender flux tube approximation in regions away from the apex. The nature of the discrepancy at the apex can be understood by expanding the right-hand side of equation (5) binomially in the neighborhood of $x = x_0$:

$$y_s(x > x_0) \approx \frac{4\pi\Delta\rho g Y}{B_0^2}(x - x_0).$$

This implies

$$\left.\frac{dy_s}{dx}\right|_{x=x_0} \approx \frac{4\pi\Delta\rho g Y}{B_0^2},$$

i.e., the curve $y_s(x)$ meets the axis at an angle. Since $y_s(x)$ represents a line of force, this will mean bending a line of force at a sharp angle. Certainly this cannot be a valid equilibrium approximation near the apex. We now present an analytical scheme for treating the field in a small region around the apex.

A two-dimensional field can be represented using a scalar function $A(x, y)$ such that

$$B_x = \frac{\partial A}{dy}, \qquad B_y = -\frac{\partial A}{\partial x}. \tag{6}$$

The field lines are given by contours of constant A. Write A as

$$A = B_0 y + A', \tag{7}$$

where the first term alone would give a constant vertical field, and the second term incorporates the effect of the field-free fluid

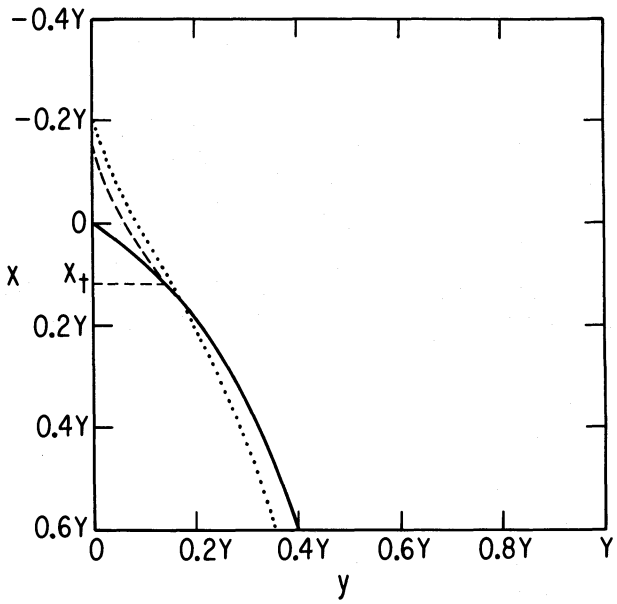

FIG. 2

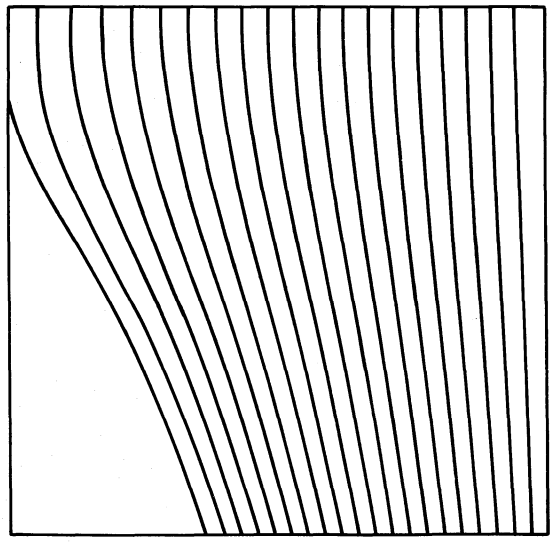

FIG. 3

FIG. 2.—The solid curve is the surface of separation as given by eq. (5) with $\Delta\rho g Y/B_0^2 = 0.118$ and $x_0 = 0$. The dotted curve is obtained numerically by an iterative procedure starting from the solid curve. The dashed curve is the plot of eq. (14) with α given by eq. (16) and matches the solid curve at the height x_t.

FIG. 3.—Distribution of field lines obtained numerically for the numerical boundary shown by the dotted curve in Fig. 2

column. We solve for a potential field in the magnetized fluid so that A satisfies

$$\frac{\partial^2 A}{\partial x^2} + \frac{\partial^2 A}{\partial y^2} = 0 \tag{8}$$

inside the magnetized fluid. Since A is constant on the boundary of separation $y_s(x)$, we can arrange that A has the constant value zero there, i.e.,

$$A(x, y_s(x)) = 0 . \tag{9}$$

If the apex is at x_1, our problem now is to find a solution of equation (8) of the form (7) within the magnetized fluid in the neighborhood of $(x_1, 0)$ such that the boundary $y_s(x)$ given by equation (9) has the following characteristics:

(i) $y_s(x) = 0$ for $x < x_1$;
(ii) $dy_s/dx = 0$ at $x = x_1$;
(iii) $y_s(x)$ increases monotonically as x increases beyond x_1;
(iv) $B^2 = (\partial A/\partial x)^2 + (\partial A/\partial y)^2$ calculated on $y_s(x)$ varies linearly with x for $x > x_1$.

The last condition ensures that equation (1) holds.

We now show that all these conditions are satisfied if we take

$$A' = -\alpha \,\mathrm{Re}\, [(x - x_1) + iy]^{3/2} . \tag{10}$$

With polar coordinates

$$q = [(x - x_1)^2 + y^2]^{1/2}, \qquad u = \arctan\left(\frac{y}{x - x_1}\right),$$

equations (7) and (10) become

$$A = B_0 q \sin u - \alpha q^{3/2} \cos \tfrac{3}{2}u . \tag{11}$$

It is easy to show that equation (11) satisfies the two-dimensional Laplace's equation (8). If (q_s, u_s) are points on the surface of separation $y_s(x)$, then we must have

$$B_0 \sin u_s - \alpha q_s^{1/2} \cos \tfrac{3}{2}u_s = 0 . \tag{12}$$

This equation is satisfied for any q_s when $u_s = \pi$, i.e., $y_s(x) = 0$ for $x < x_1$. For $x > x_1$, note that B^2 is given by

$$B^2 = \left(\frac{\partial A}{\partial q}\right)^2 + \left(\frac{1}{q}\frac{\partial A}{\partial u}\right)^2$$
$$= B_0^2 + \tfrac{9}{4}\alpha^2 q + 3\alpha B_0 q^{1/2} \sin \tfrac{1}{2}u .$$

On the boundary specified by equation (12), B^2 becomes

$$B^2|_s = B_0^2 + 3\alpha^2 q_s \cos u_s + \tfrac{3}{4}\alpha^2 q_s . \tag{13}$$

If we now transform back to Cartesian coordinates, then equations (12) and (13) give, for $x > x_1$,

$$y_s(x > x_1) = \frac{\alpha}{B_0}(x - x_1)^{3/2}\left\{1 + \frac{3}{8}\left(\frac{\alpha}{B_0}\right)^2 (x - x_1) + O\left[\left(\frac{\alpha}{B_0}\right)^4 (x - x_1)^2\right]\right\}, \tag{14}$$

$$B^2(x > x_1)|_s = B_0^2\left\{1 + \frac{15}{4}\left(\frac{\alpha}{B_0}\right)^2 (x - x_1) + O\left[\left(\frac{\alpha}{B_0}\right)^4 (x - x_1)^2\right]\right\} . \tag{15}$$

Now it is easy to see that requirements (i)–(iv) are satisfied, provided that the higher order terms can be neglected. From equations (1), (3), and (15), we conclude that

$$\alpha^2 = \frac{32\pi}{15}\Delta\rho g . \tag{16}$$

The condition for higher order terms to be neglected now becomes

$$\frac{15}{4}\left(\frac{\alpha}{B_0}\right)^2 (x - x_1) \ll 1 ,$$

i.e.,

$$(x - x_1) \ll \frac{B_0^2}{8\pi\Delta\rho g} . \tag{17}$$

This inequality gives the dimension of the region around $(x_1, 0)$ for which equation (11) gives a solution satisfying all the necessary

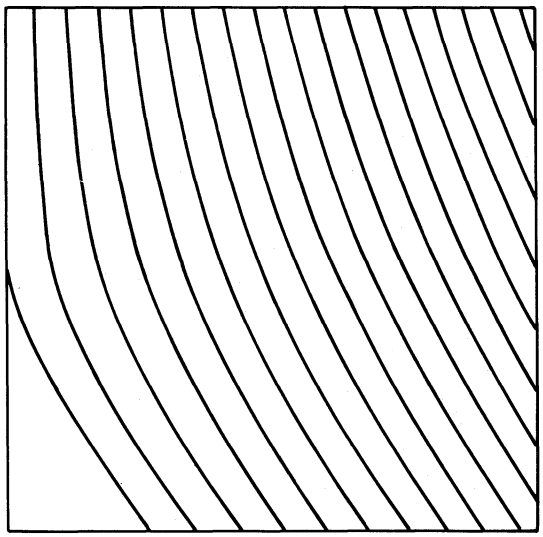

FIG. 4.—Contours of constant A (i.e., field lines) as given by eq. (11). We use the same α as used for the dashed curve in Fig. 2. However, this figure is magnified by a factor of 2 compared with Figs. 2 and 3, and shows only the region near the apex.

requirements. Figure 4 shows the lines of force as given by equation (11). A noteworthy aspect of the problem is that the boundary below the apex opens up with a 3/2 power dependence as shown by equation (14).

We now have a quite satisfactory situation. We have developed a scheme for studying the behavior of the system near the apex, whereas the behavior away from the apex can be studied by the slender flux tube approximation. The dashed curve in Figure 2 shows $y_s(x)$ as given by equation (14) (to second term), which is superposed to match the slender flux tube solution. Let x_t be the height at which one curve can be made to touch the other. Since both $y_s(x)$ and dy_s/dx at x_t obtained from either equation (5) or equation (14) have to be the same, we have

$$\frac{4\pi\Delta\rho g Y}{B_0}(x_t - x_0) \approx \alpha(x_t - x_1)^{3/2}, \qquad \frac{4\pi\Delta\rho g Y}{B_0} \approx \frac{3}{2}\alpha(x_t - x_1)^{1/2},$$

where we keep only the leading terms to get a rough estimate. From these two equations, the amount by which the position of the apex is raised on relaxing the slender flux tube approximation is

$$(x_0 - x_1) \approx \frac{1}{2}(x_t - x_0) \approx \frac{10\pi\Delta\rho g Y^2}{9B_0^2}. \tag{18}$$

In order that the higher order terms in equation (15) can be neglected over this region, we have, from (17) and (18),

$$\frac{\Delta\rho g Y}{B_0^2} \ll \left(\frac{9}{80}\right)^{1/2}\frac{1}{\pi}. \tag{19}$$

When this condition is satisfied, we are justified in solving the problem in the two different ways near the apex and away from the apex, and then matching the two solutions. For the conditions of the solar photosphere, with $B_0 = 3000$ G and $\Delta\rho = 10^{-7}$ g cm^{-3}, inequality (19) implies

$$Y \ll 3000 \text{ km}.$$

Thus the maximum limit of Y is much larger than dot diameters.

b) *Three-dimensional Case*

Let us use cylindrical coordinates with z-axis in the vertical direction (z increasing downward). We look for axisymmetric solutions with

$$r = r_s(z)$$

as the boundary of separation over which equation (1) is satisfied. Assume that the field becomes vertical at $r = R$ and the *slender flux tube approximation* holds. In the place of equation (2), we have in three dimensions

$$B(z)[R^2 - r_s^2(z)] = B_0 R^2. \tag{20}$$

The internal and external pressures are as usual given by

$$p_i = p_i g z + c_i, \qquad p_e = \rho_e g z + c_e. \tag{21}$$

Combining equations (1), (20), and (21), we have

$$\frac{r_s(z > z_0)}{R} = \left\{1 - \left[1 + \frac{8\pi\Delta\rho g R}{B_0^2}\left(\frac{z}{R} - \frac{z_0}{R}\right)\right]^{-1/2}\right\}^{1/2}, \tag{22}$$

where $\Delta\rho = \rho_i - \rho_e$, and $z = z_0$ is the apex. The relationship among z_0, c_i, and c_e is

$$\Delta\rho g z_0 = \frac{B_0^2}{8\pi} + c_e - c_i . \tag{23}$$

Equation (22) prescribes the surface of separation as given by slender flux tube approximation. In the neighborhood of $z = z_0$,

$$\left[\frac{r_s(z > z_0)}{R}\right]^2 \approx \frac{4\pi\Delta\rho g}{B_0^2}(z - z_0) ,$$

so that

$$\left.\frac{dr_s}{dz}\right|_{z=z_0} \approx R\left[\frac{\pi\Delta\rho g}{B_0^2(z - z_0)}\right]^{1/2} .$$

Thus we see that the surface is of parabolic shape, meeting the central axis perpendicularly. To get around this unphysical result, we have to relax the slender flux approximation.

The problem of constructing a local solution around the apex becomes much more complicated when we go from two to three dimensions. If we introduce a vector potential

$$A = A(r, z)\hat{e}_\theta ,$$

then components of the magnetic field $\boldsymbol{B} = -\nabla \times \boldsymbol{A}$ are given by

$$B_r = -\frac{\partial A}{\partial z}, \qquad B_z = \frac{1}{r}\frac{\partial}{\partial r}(rA) . \tag{24}$$

It is easy to show that the lines of force will lie on surfaces of constant rA. We now seek a solution of the form

$$A = \tfrac{1}{2}B_0 r + A' , \tag{25}$$

where the first term alone would give a constant vertical field B_0. For a potential field in the magnetized fluid,

$$\nabla \times \boldsymbol{B} = 0 ,$$

i.e.,

$$\frac{\partial^2 A}{\partial z^2} + \frac{\partial}{\partial r}\left[\frac{1}{r}\frac{\partial}{\partial r}(rA)\right] = 0 \tag{26}$$

has to hold. We can again arrange that A is zero on the surface of separation, i.e.,

$$A(z, r_s(z)) = 0 . \tag{27}$$

As in the case of two dimensions, our problem now is to obtain a solution of equation (26) of the form (25) around the apex $z = z_1$ in such a way that the boundary $r_s(z)$ given by equation (27) again satisfies the four criteria:

(i) $r_s(z) = 0$ for $z < z_1$;
(ii) $dr_s/dz = 0$ at $z = z_1$;
(iii) $r_s(z)$ increases monotonically as z increases beyond z_1;
(iv) $B^2 = (B_r)^2 + (B_z)^2$ calculated on $r_s(z)$ varies linearly with z for $z > z_1$.

If we make a coordinate transformation,

$$q = [(z - z_1)^2 + r^2]^{1/2}, \qquad u = \tan^{-1}\left(\frac{r}{z - z_1}\right)$$

[q and u are analogous to polar coordinates in the (r, z)-plane], then equation (26) becomes

$$\frac{1}{q}\frac{\partial}{\partial q}\left(q\frac{\partial A}{\partial q}\right) + \frac{1}{q^2}\frac{\partial^2 A}{\partial u^2} + \frac{\partial}{\partial q}\left(\frac{A}{q}\right) + \frac{\cos u}{q^2}\frac{\partial}{\partial u}\left(\frac{A}{\sin u}\right) = 0 . \tag{28}$$

Consider an exact solution of this equation

$$A' = -\alpha q^2\left\{\frac{\cos^3 u + 1}{\sin u} - 3\sin u - \frac{3}{2}\sin 2u \ln\left[\frac{q}{q_0}(1 - \cos u)\right]\right\}, \tag{29}$$

where q_0 is a constant having the dimension of length. This solution is singular for $u = 0$. However, $u = 0$ corresponds to the central

axis of the field-free fluid and lies outside the domain over which we want to solve equation (28). From equation (25), the full solution is

$$A = \tfrac{1}{2}B_0 q \sin u + A' , \tag{30}$$

with A' given by equation (29). Contours of constant $rA = q \sin uA$ are shown in Figure 5. It is easy to see that $A = 0$ for $u = \pi$, i.e., $r_s(z) = 0$ for $z < z_1$. To find the boundary for $z > z_1$, we transform equation (29) back to (r, z) coordinates and expand in the neighborhood of $u = 0$, where $r/(z - z_1) \ll 1$. This yields

$$A'(z > z_1) = -\frac{\alpha(z - z_1)^3}{r}\left\{2 - \frac{3}{2}\left(\frac{r}{z - z_1}\right)^2 - 3\left(\frac{r}{z - z_1}\right)^2 \ln\left[\frac{r^2}{2q_0(z - z_1)}\right] + O\left[\left(\frac{r}{z - z_1}\right)^4\right]\right\} . \tag{31}$$

The boundary $r_s(z)$, obtained on combining equations (27), (30), and (31), is

$$r_s(z > z_1) = 2\left(\frac{\alpha}{B_0}\right)^{1/2}(z - z_1)^{3/2}\left\{1 - \frac{3}{2}\frac{\alpha}{B_0}(z - z_1) - 3\frac{\alpha}{B_0}(z - z_1)\ln\left[\frac{2\alpha}{B_0}\frac{(z - z_1)^2}{q_0}\right] + \cdots\right\} . \tag{32}$$

This expression implies that conditions (ii) and (iii) are satisfied. It is straightforward to show that $B^2 = (B_r)^2 + (B_z)^2$ on the surface of separation is

$$B^2(z > z_1)|_s = B^2\left\{1 + 27\frac{\alpha}{B_0}(z - z_1) + 12\frac{\alpha}{B_0}(z - z_1)\ln\left[\frac{2\alpha}{B_0}\frac{(z - z_1)^2}{q_0}\right] + O\left[\left(\frac{\alpha}{B_0}\right)^2(z - z_1)^2\right]\right\} . \tag{33}$$

Thus we see that, among terms to the leading order, there is a logarithmic term in addition to the linear term. Figure 6 illustrates the nature of this logarithmic term. It becomes negative in a small region near $z = z_1$. However, this region can be made arbitrarily small by making q_0 smaller and smaller. In the limit of $q_0 \to 0$, we thus have a linear term along with another term starting to increase monotonically arbitrarily close to the apex.

To summarize, we have obtained a completely satisfactory two-dimensional solution near the apex and a three-dimensional solution which possesses most of the desirable characteristics. Equations (14) and (32) imply that, in both cases, the field-free fluid column opens up with a power law of 3/2. It seems possible that a 3/2 power law may represent a universal characteristic of such systems.

III. STEADY-FLOW SOLUTIONS FOR INCOMPRESSIBLE FLUIDS

In the last section, we considered the equilibrium configurations of field-free fluid columns surrounded by magnetized fluids. In this paper we do not address the extremely complicated problem of stability of such configurations. It is well known from both theoretical and observational considerations that a variety of wave modes exist in systems where we have field-free and magnetized fluids side by side. The waves in sunspots have been investigated by several authors (Nye and Thomas 1974; Antia, Chitre, and

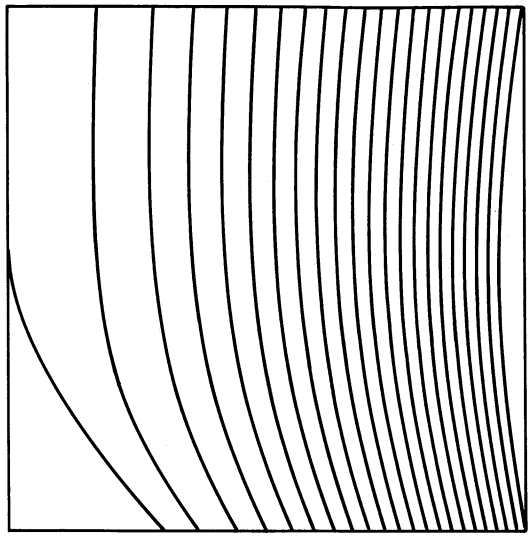

FIG. 5

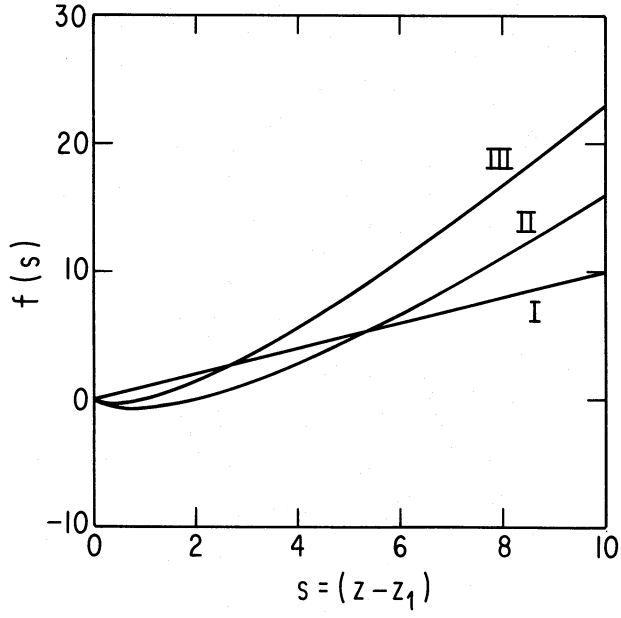

FIG. 6

FIG. 5.—Contours of constant rA as given by eq. (30). With the side of the diagram as the unit of length, we have $\alpha/B_0 = 0.1$ (in units of inverse length) and $q_0 = 1.0$.

FIG. 6.—An illustration of the logarithmic term in eq. (33). *Curve I*: $f(s) = s$. *Curve II*: $f(s) = s \log (s/2)$. *Curve III*: $f(s) = s \log s$

Gokhale 1978; Antia and Chitre 1979; Thomas and Scheuer 1982). We have already mentioned Parker's work on oscillations of a field-free fluid slab between regions of vertical magnetic fields (Parker 1979*c*). However, most of these analyses are linear and do not throw much light on the amplitudes of the oscillations. Most probably it is possible for oscillations to take place about the equilibrium configurations we have derived here. However, unless the oscillations have very large amplitudes, our equilibrium solutions can be regarded as mean configurations good enough for our purpose.

We want to study a different aspect of the problem. Assume that the top of the surrounding fluid (i.e., the surface S in Fig. 1) is at a horizontal level $z = 0$, so that c_e in equation (21) is zero. The constant c_i is a measure of the push from the bottom inside the field-free fluid. It follows from equation (23) that an increase in c_i makes z_0 smaller (i.e., makes the apex rise). Since z_0 must be positive for equilibrium, we must have

$$c_i < \frac{B_0^2}{8\pi} . \tag{34}$$

When $c_i = B_0^2/8\pi$, we have $z_0 = 0$, i.e., the apex of the column just touches the free surface. Actually z_0 is the position of the apex in the *slender flux tube approximation* and the real apex is a little bit higher than that. Hence the apex would touch the free surface for a slightly smaller value of c_i. However, we neglect those fine details in the present analysis. From equation (22) it follows that $r_s(z)$ depends only on $(z - z_0)$, but not on z or z_0 explicitly. Hence, wherever the apex of the tapering column may be, the general structure of the column below the apex is the same. When the field-free liquid is pressurized more from the bottom, the tapering fluid column undergoes only an upward translation, without changing its shape or structure.

Consider the situation when the field-free fluid has pressure enough to burst into the open space above. Under steady conditions we have the Bernoulli equation

$$\tfrac{1}{2}\rho_i v^2 + p_i - \rho_i g z = c_i \tag{35}$$

along the slender flux tube. The justification for using the same constant of integration c_i is that, in the limit $v \to 0$, equation (35) reduces to (21). The conservation of fluid implies that

$$F = -v r_s^2(z) \tag{36}$$

is a constant. The minus sign makes sure that F is positive for upward flows. Hence, from (20),

$$B = B_0\left(1 + \frac{F}{R^2 v}\right)^{-1} ,$$

and we further have

$$p_i = p_e + \frac{B^2}{8\pi}$$

$$= \rho_e g z + \frac{B_0^2}{8\pi(1 + F/R^2 v)^2} .$$

Substituting this in equation (35), we obtain

$$\frac{B_0^2}{8\pi} H\left(\frac{F/R^2}{B_0/(4\pi\rho_i)^{1/2}} ; v'\right) = c_i' + \Delta\rho g z , \tag{37}$$

where

$$c_i' = c_i - \frac{B_0^2}{8\pi} \tag{38}$$

and

$$v' = \frac{v}{B_0/(4\pi\rho_i)^{1/2}} \tag{39}$$

is the velocity in units of $B_0/(4\pi\rho_i)^{1/2}$ [which is $(\rho_e/\rho_i)^{1/2}$ times the Alfvén speed in the undisturbed fluid], and where the function $H(b; v')$ is defined as

$$H(b; v') = v'^2\left[1 + \frac{1}{(v' + b)^2}\right] - 1 . \tag{40}$$

Figure 7 shows the nature of the relation between v' and the function $H(b; v')$ for different values of the parameter b. From equation (37) it also follows that $H(b; v')$ is essentially a measure of z, so that from Figure 7 we conclude that there can be two solutions of v' for every value of z, other parameters being fixed. One of the solutions lies on the upper parts of curves in Figure 7 (*dashed curves*) and increases monotonically with z, implying that the radius of the field-free fluid column decreases with depth. This is contrary to the physical situation treated here. The physical solutions represented by the solid curves have smaller velocities and

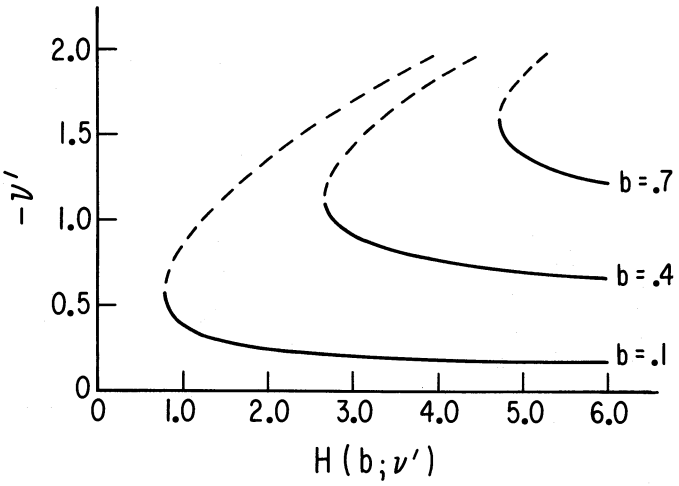

FIG. 7

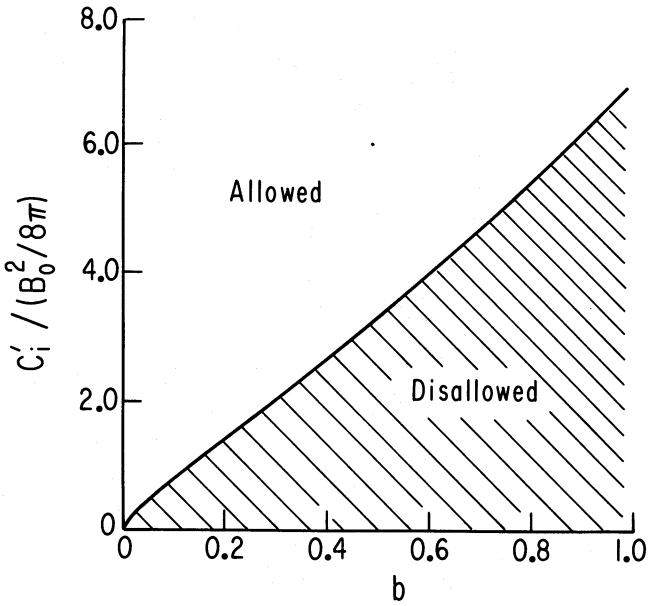

FIG. 8

FIG. 7.—Plot of v' versus $H(b; v')$ as given by eq. (40) for three values of b

FIG. 8.—The region of parameter space (for incompressible fluids) which allows steady-flow solutions. The region that does not allow such solutions is shaded, the boundary between the two regions being given by eq. (42).

larger radii as we go down. The two solutions converge at a point where $H(b; v')$ has a minimum value $H_{\min}(b)$. We want a solution to exist for all positive values of z, including $z = 0$. It follows from equation (37) that this is possible only if

$$\frac{c_i'}{B_0^2/8\pi} > H_{\min}(b) \, . \tag{41}$$

We can obtain an expression for $H_{\min}(b)$ from the fact that, at the stationary point,

$$\left(\frac{\partial H}{\partial v'}\right)_b = 0 \, .$$

Using this condition, it follows from equation (40) that

$$H_{\min}(b) = b^2 + 3b^{4/3} + 3b^{2/3} \, . \tag{42}$$

In Figure 8 we indicate the allowed regions for physical solutions in the $[b, c_i'/(B_0^2/8\pi)]$-plane. The allowed and disallowed regions are separated by the $H_{\min}(b)$-curve. Remembering that b is a measure of flow and c_i' is a measure of excess pressure of the field-free fluid, we can conclude from Figure 8 that, for a stronger flow, the minimum value of excess pressure has to be higher. For vanishingly small flows, the minimum value of c_i' goes to zero. In other words, in order for a steady-flow solution to exist, equation (38) implies

$$c_i > \frac{B_0^2}{8\pi} \, . \tag{43}$$

This condition is clearly consistent with condition (34) for static equilibrium.

If the excess pressure is such that c_i just exceeds the critical value $B_0^2/8\pi$, then only a weak flow can take place. A larger c_i makes stronger flows possible. However, the strength of an actual flow realized in a particular situation must be determined by the details of the system, such as the amount of fluid available to maintain the flow. As more and more fluid gushes out, the flow may tend to become weaker. The complete problem is an extremely complicated time-dependent affair, which we do not venture to study here. We believe that the equilibrium and steady-flow solutions presented here throw some light on the general behavior of the system.

IV. SOLUTIONS FOR POLYTROPIC ATMOSPHERES

a) Equilibrium Configurations

We now show that the same qualitative considerations hold for compressible gases in a polytropic atmosphere. The temperature of such an atmosphere varies linearly with depth, i.e. the temperatures within the magnetized gas and within the field-free gas can be written respectively as

$$T_e = \beta z + T_f \, , \qquad T_i = \beta z + T_f + T_d \, , \tag{44}$$

where T_f is the temperature at the free surface where magnetic pressure suddenly drops, and T_d is the temperature enhancement within the field-free gas. We take the same temperature gradient both inside and outside to make the problem tractable. The perfect-gas law,

$$p = \mathcal{R}\rho T \,, \tag{45}$$

is supposed to hold. The hydrostatic equation for the external gas,

$$\frac{dp_e}{dz} = \rho_e g$$

$$= \frac{p_e g}{\mathcal{R}(\beta z + T_f)} \,,$$

can be integrated to

$$p_e = \frac{\mathcal{R}^\alpha}{K_e^{\alpha-1}} (\beta z + T_f)^\alpha \,, \tag{46}$$

where

$$\alpha = \frac{g}{\mathcal{R}\beta} \tag{47}$$

is the polytropic index and the constant of integration K_e is chosen such that

$$\frac{p_e}{\rho_e^{\alpha/(\alpha-1)}} = K_e \,. \tag{48}$$

Here ρ_e is the external density given by

$$\rho_e = \frac{\mathcal{R}^{\alpha-1}}{K_e^{\alpha-1}} (\beta z + T_f)^{\alpha-1} \,.$$

Similar expressions hold for the pressure and density of the field-free gas with, in general, a different constant K_i, i.e.,

$$p_i(z > z_0) = \frac{\mathcal{R}^\alpha}{K_i^{\alpha-1}} (\beta z + T_f + T_d)^\alpha \,. \tag{49}$$

We again take $z = z_0$ to be the position of the apex of the tapering column of field-free gas. From equations (1), (46), and (49), the magnetic field is given by

$$B(z > z_0) = \left\{ 8\pi \frac{\mathcal{R}^\alpha}{K_e^{\alpha-1}} \left[Q(T_d)(\beta z + T_f + T_d)^\alpha - (\beta z + T_f)^\alpha \right] \right\}^{1/2} \,, \tag{50}$$

where

$$Q(T_d) = \left(\frac{K_e}{K_i} \right)^{\alpha-1}$$

is a dimensionless quantity of the order of unity. If more heat is deposited in the field-free fluid to raise T_d, obviously K_i increases so that $Q(T_d)$ is a function of T_d. The surface of separation in the *slender flux tube approximation* is

$$\frac{r_s(z)}{R} = \left(1 - \frac{B_0}{B} \right)^{1/2} \,,$$

with B given by equation (50). Since $B = B_0$ at $z = z_0$, from equation (50) we have

$$B_0 = \left\{ 8\pi \frac{\mathcal{R}^\alpha}{K_e^{\alpha-1}} \left[Q(T_d)(\beta z_0 + T_f + T_d)^\alpha - (\beta z_0 + T_f)^\alpha \right] \right\}^{1/2} \,. \tag{51}$$

If we make a binomial expansion of the pressures just below the apex, we can write

$$\frac{B^2}{8\pi} = \frac{B_0^2}{8\pi} + \frac{\alpha\beta\mathcal{R}^\alpha}{K_e^{\alpha-1}} (z - z_0)[Q(T_d)(\beta z_0 + T_f + T_d)^{\alpha-1} - (\beta z_0 + T_f)^{\alpha-1}] + O[\beta^2 (z - z_0)^2] \,,$$

i.e., we can approximate the magnetic pressure to increase linearly for some distance, and the schemes developed in § II to treat regions around the apex are applicable to compressible gases also. The 3/2 power law may indeed be a quite general law!

From equation (51), we obtain

$$\frac{dT_d}{dz_0} = -\beta\left[1 - \frac{1}{Q(T_d)}\left(\frac{\beta z_0 + T_f}{\beta z_0 + T_f + T_d}\right)^{\alpha-1}\right] - \frac{1}{\alpha Q(T_d)}(\beta z_0 + T_f + T_d)\frac{dQ}{dz_0}. \tag{52}$$

This equation describes how z_0 decreases (i.e., the apex rises) as T_d is increased. Finally we reach the critical position $z_0 = 0$ when

$$M(T_d) = 1 + \lambda,$$

where

$$M(T_d) = Q(T_d)\left(1 + \frac{T_d}{T_f}\right)^{\alpha} \tag{53}$$

and

$$\lambda = \frac{K_e^{\alpha-1}B_0^2}{8\pi(\mathscr{R}T_f)^{\alpha}} \tag{54}$$

is the ratio of the magnetic pressure to the gas pressure (i.e., the inverse of plasma β) at the free surface. Thus we conclude that, if a static equilibrium solution is to exist, then we must have

$$M(T_d) < 1 + \lambda. \tag{55}$$

In the case of compressible gases, however, the successive equilibrium configurations for increasing $M(T_d)$ cannot be obtained by simple vertical displacements of the tapering column as in the case of incompressible fluids.

b) Steady Adiabatic Upward Flow

We now want to study a steady flow as in the previous case. Consider an adiabatic flow such that the pressure and the density at any point are related by

$$\frac{p_i}{\rho_i^{\gamma}} = K_i', \tag{56}$$

where K_i' is a constant. Using this isentropic condition, the equation of motion

$$\rho_i v\frac{dv}{dz} = -\frac{dp_i}{dz} + \rho_i g$$

can be integrated to give

$$\tfrac{1}{2}v^2 + \alpha' K_i'\rho_i^{\gamma-1} - gz = C. \tag{57}$$

Here C is the constant of integration, and

$$\alpha' = \frac{\gamma}{\gamma - 1}. \tag{58}$$

The equation of continuity implies that

$$\mathscr{F} = -\rho_i r_s^2(z)v \tag{59}$$

is a constant.

To proceed further, we make two assumptions. First, since our system is embedded in an atmosphere where convection is taking place in any field-free region, we assume the convective condition that the actual temperature gradient is equal to the adiabatic gradient. This condition is equivalent to setting

$$\alpha' = \alpha \tag{60}$$

(see Appendix). The second assumption is that, for vanishingly small flows, the internal solution tends to an equilibrium solution for which

$$K_i' = K_i.$$

This assumption demands that the constant of integration C appearing in equation (57) is given by

$$C = \alpha\mathscr{R}(T_f + T_d). \tag{61}$$

From equations (1), (20), and (46), we now obtain an expression for the internal pressure

$$p_i = \frac{\mathscr{R}^{\alpha}}{K_e^{\alpha-1}}(\beta z + T_f)^{\alpha} + \frac{B_0^2}{8\pi[1 - r_s^2(z)/R^2]^2}$$
$$= \frac{\mathscr{R}^{\alpha}T_f^{\alpha}}{K_e^{\alpha-1}}(1+\xi)^{\alpha}\left[1 + \frac{\lambda}{(1+\xi)^{\alpha}(1-u^2)^2}\right], \tag{62}$$

where

$$u = \frac{r_s(z)}{R}$$

and

$$\xi = \frac{\beta z}{T_f} .$$

Equations (56)–(62) can now be combined to give, after some straightforward algebraic manipulation,

$$\frac{Su^{-4}}{(1+\xi)^{2\alpha-1}\{1+\lambda/[(1+\xi)^{\alpha}(1-u^2)^2]\}^{(2\alpha-2)/\alpha}} = Q^{1/\alpha}(T_d)\left(\frac{1+\xi+T_d/T_f}{1+\xi}\right) - \left[1+\frac{\lambda}{(1+\xi)^{\alpha}(1-u^2)^2}\right]^{1/\alpha}, \tag{63}$$

where

$$S = \frac{(\mathscr{F}/R^2)^2 K_e^{2(\alpha-1)}}{2\alpha Q^{1/\alpha}(T_d)(\mathscr{R}T_f)^{2\alpha-1}} .$$

This equation can be thought of as an implicit solution for the dependent variable $u = r_s(z)/R$ in terms of the independent variable $\xi = \beta z/T_f$, when the parameters $Q(T_d)$, T_d/T_f, S, and λ are given. Once we have obtained a solution for $r_s(z)$, we can calculate p_i by using equation (62), and consequently ρ_i by using equation (56). When $r_s(z)$ and ρ_i are known, we can obtain v from equation (59).

We now try to figure out which regions of parameter space allow steady-flow solutions. If we put $\xi = 0$ in equation (63), then we obtain the following equation for $u_f = r_s(0)/R$ at the surface:

$$\frac{Su_f^{-4}}{[1+\lambda/(1-u_f^2)^2]^{(2\alpha-2)/\alpha}} = M^{1/\alpha}(T_d) - \left[1+\frac{\lambda}{(1-u_f^2)^2}\right]^{1/\alpha} . \tag{64}$$

For a steady flow, u_f must have a real value at the surface lying in the range (0, 1). Consider the results for a particular value of λ, say $\lambda = 3$. We take $\gamma = 5/3$ so that $\alpha = 5/2$. For any given S, we can now solve equation (64) to obtain values of u_f for different values of $M(T_d)$. Figure 9 shows such solutions for three given values of S. It is seen that no real solutions in the range (0, 1) exist when $M(T_d)$ is less than the critical value $M_c(T_d) = 4$ given by inequality (55). For a given value of S, solutions are possible only when $M(T_d)$ is larger than a minimum value $M_{\min}(T_d, S, \lambda = 3)$. For larger values of $M(T_d)$, there exist two solutions. The upper solid curve in Figure 9 implies that u_f increases with $M(T_d)$, i.e., the mouth of the flow opens more as we increase the overpressure below. This is the physical solution, while the lower dashed curve is unphysical.

We estimate $M_{\min}(T_d, S, \lambda)$ in the following way. At the stationary point,

$$\left(\frac{\partial M}{\partial u_f}\right)_{S,\lambda} = 0 .$$

Using this condition (64) leads to

$$\frac{\lambda}{\alpha}\left[1+\frac{\lambda}{(1-u_{st})^2}\right]^{(\alpha-1)/\alpha} = S\frac{(1-u_{st}^2)^3}{u_{st}^6} + \frac{[(2\alpha-2)/\alpha]\lambda S}{u_{st}^4[1+\lambda/(1-u_{st}^2)^2]} , \tag{65}$$

where u_{st} is the value of u_f at the stationary point. After u_{st} has been obtained from equation (65), it can be substituted back in

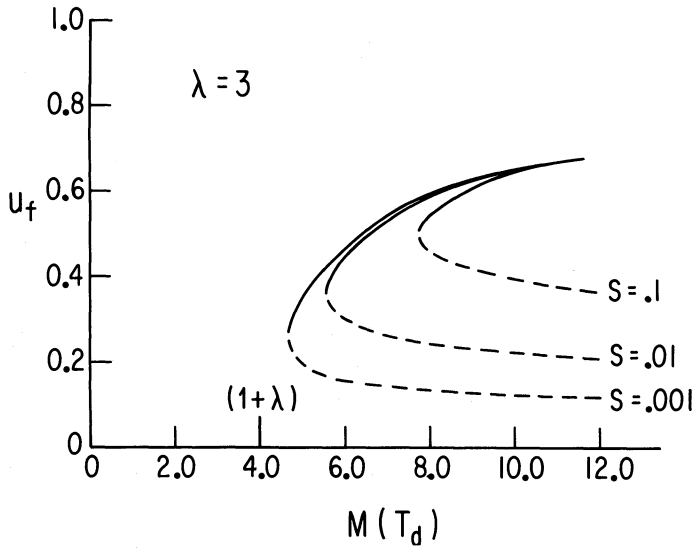

FIG. 9.—Plot of u_f vs. $M(T_d)$ as given by eq. (64) for three values of S and a fixed value of $\lambda = 3$

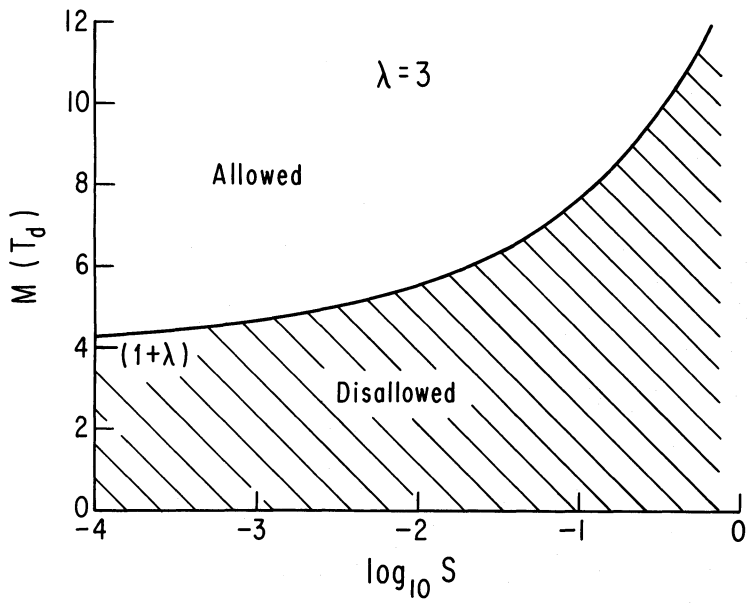

FIG. 10.—The region of parameter space (for compressible fluids with $\lambda = 3$) which allows steady-flow solutions. The region not allowing such solutions is shaded.

equation (64) to give $M_{\min}(T_d, S, \lambda)$. Figure 10 shows the allowed region for flow solutions in a $[M(T_d), \log_{10} S]$ plot for $\lambda = 3$ (obtained numerically). For other values of λ, we expect the same qualitative behavior with

$$M_c(T_d) = 1 + \lambda .$$

We conclude that the general features of a magnetic valve in an incompressible fluid are essentially the same as those of a magnetic valve in a polytropic atmosphere. Given that λ is a fixed parameter for a particular system, the nature of the flow is determined by two parameters: one of them, $M(T_d)$, is a measure of internal overpressure, and the other, S, a measure of the amount of gas available for flow.

V. DISCUSSION

We are now in a position to consider the significance of our formal calculations for an actual sunspot. If a sunspot is really a composite object as envisaged by Parker (1979*b*), then certainly there are regions of field-free gas intruding into the sunspot. These field-free gas pockets would take up shapes of tapering columns (as shown in Fig. 1*a*) within which convective transport of heat may go on. Because of the limited transverse dimensions, convection in these pockets may not be as efficient as in the outer convection zone. We expect such regions to carry a fraction v of the heat flux F_H carried by the convection zone ($0 < v < 1$). When this flux vF_H reaches the neighborhood of the apex, it can diffuse in the surrounding stable atmosphere only by radiation. If κ is the Rosseland mean opacity, the mean free path of a photon is $(\rho\kappa)^{-1}$ and the coefficient of photon diffusivity is given by

$$D \approx \frac{c}{3\rho\kappa} .$$

In any diffusive process, the linear dimension over which diffusion takes place in time t is $(Dt)^{1/2}$, i.e., the distance through which photons diffuse from the sides of the field-free column in time t is

$$s \approx at^{1/2} ,$$

where

$$a = \left(\frac{c}{3\rho\kappa}\right)^{1/2} .$$

Using a model of the solar convection zone (Spruit 1974), we find the values of a shown in Table 1 for three depths below the

TABLE 1

VALUE OF a AS A FUNCTION OF DEPTH

Depth (km)	a (cgs units)
33	1.01×10^8
10^3	1.21×10^6
4.68×10^3	3.49×10^4

photosphere. Thus photons can diffuse through 1000 km in 1 s at the top of the photosphere, but they diffuse through only a fraction of a kilometer in 1 s when we go to a depth of nearly 5000 km. If the apex of the field-free column is more than 1000 km under the photosphere, the radiative diffusion is rather inefficient, and the heat carried by convection may pile up, causing the column to rise. The above arguments may be somewhat too sketchy to be taken as an infallible "proof" that things are really this way, but they make it clear that such a scenario is highly plausible. Until we have a fairly complete understanding of magneto-convection in a stratified atmosphere, we cannot hope to do any better.

To make a very rough estimate of the rate of rise of the column, let us assume that flux vF_H is absorbed in the last l km below the apex. Then the rate of temperature rise would be

$$\left|\frac{\partial T}{\partial t}\right| \approx \frac{vF_H}{\rho l c_p}.$$

We know from equation (52) that $|dT_d/dz_0|$ is a fraction v' of β $(0 < v' < 1)$. Hence the rate of rise of the apex is

$$\left|\frac{dz_0}{dt}\right| \approx \frac{vF_H}{v'\beta\rho l c_p}.$$

Let us take $l \approx 10^3$ km, $\beta = 5$ K km^{-1}. Using the values of ρ and c_p at depths of 10^3 km and 4.68×10^3 km (Spruit 1974), we find $|dz_0/dt|$ to be $3.2 \times 10^{-2}(v/v')$ km s^{-1} and $1.2 \times 10^{-3}(v/v')$ km s^{-1}, respectively, for the two depths. Thus the speed of ascent is negligible compared with the sound speed, and the field-free gas column can be assumed to be in dynamical equilibrium with the surroundings at every stage of the ascent. This justifies the use of our equilibrium solutions to describe the successive stages of evolution. Taking $v/v' \approx 1$, we find that an apex at a depth of 10^3 km would rise about 100 km in an hour, which seems reasonable considering the sizes and lifetime of typical sunspots.

As the apex rises higher and the radiative diffusion becomes more effective, the region around the apex has less sharply defined boundaries. We came to the conclusion in §§ III and IV that the field-free gases ultimately give rise to upward-moving jets, albeit, on the basis of our calculations omitting radiative transfer and assuming that the surrounding magnetic pressure drops suddenly. Owing to the idealized nature of our calculations, we cannot assert conclusively on theoretical grounds alone that there will be such jets in the umbra. However, if the observations of upward gas motions in umbral dots are correct (Kneer 1973), then it seems that there do indeed exist such jets as are hinted at by our rather idealized considerations. From Figure 7 we see that the velocities with which the field-free gas ultimately emerges are of the order of the Alfvén speed in the surrounding magnetized gas. This is consistent with the fact that the Alfvén speed in a sunspot umbra is of the order of 10 km s^{-1}, whereas Kneer (1973) observed upward velocities of about 3 km s^{-1}.

Figure 11*a* shows the formation of a jet of field-free gas pushing open the *magnetic valve* and giving rise to an umbral dot. Since we are dealing with a complex three-dimensional system, different field-free gas pockets under the surface may be connected in complicated ways. When one of them reaches the photosphere, a flow begins. As gas flows out of this pocket, there may be flows of gas from nearby pockets, as indicated in Figure 11*a* by the broken arrows. Remember that there may be complex connections in three dimensions not shown in our two-dimensional figure. As the nearby pockets are evacuated, their apices may become lowered, leaving the magnetic field more room to expand. This may reduce the magnetic pressure around the neck of the flow path and trigger an instability. As more gas comes out, the magnetic pressure around the neck drops, and as the magnetic pressure drops, it becomes easier for the gas to maintain the flow path. We still understand too little about subsurface conditions in sunspots to make any theoretical estimate of how much gas has to flow out before the *magnetic valve* closes again. However, we can get that information from observations of umbral bright dots. Kneer's observation of an upward velocity of 3 km s^{-1} (Kneer 1973) and a lifetime of half an hour imply that the gas flowing up through one umbral dot during its lifetime would occupy, under photospheric conditions, a cylinder of height 5000 km and cross-sectional area equal to the dot area. The dimensions of such a hypothetical cylinder are considerably smaller than those of a large sunspot.

Given the fact that the penumbral magnetic field is inclined to the vertical, the field-free gas probably takes up configurations as shown in Figure 11*b*. Consequently, we expect jets inclined in a radially outward direction with respect to the center of the sunspot. If penumbral grains are just such jets observed at an inclination, then we have a natural explanation of the radially elongated shapes of the grains. The magnetic field in the penumbra is pressurized by the surrounding photosphere. As more field-free gas flows up and evacuates regions inside the penumbra, the surrounding photospheric pressure may induce inward motions by pushing the penumbra to fill up the evacuated regions and thus produce the observed inward drift of the penumbral grains (Muller 1973*a*, 1976). This is, obviously, a very qualitative picture. We still have little understanding of the processes that create sunspots or maintain

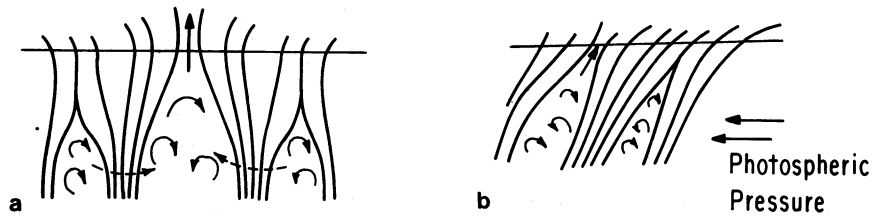

FIG. 11.—A schematic sketch of how a sunspot field may look. (*a*) An umbral dot with an indication of gas flowing from nearby field-free pockets. (*b*) The probable appearance of a penumbral grain with the external photosphere exerting pressure.

them for days. Probably a better understanding of these processes will be necessary for a satisfactory quantitative account of the inward drift of penumbral grains.

This paper is a preliminary investigation of a very complex physical system. In this first exploratory study, we have not considered many aspects of the problem which can be suitable points of departure for future research. The question of stability of our solutions is a difficult and intriguing question. In order to build a more realistic model of the fine structures of sunspots, it is necessary to couple the dynamical equations with equations of heat transfer. The assumption of magnetic pressure dropping abruptly also has to be relaxed. If umbral dots and penumbral grains are really jets of field-free gas, then they would deposit momentum and energy in the atmosphere overlying the sunspot. It would be interesting to study the effects of this momentum and energy deposition, and to consider whether this can, in any way, be related to other dynamical phenomena such as the Evershed flow. Some of these issues are currently under investigation. We hope to be able to present the results in a future paper.

It is a great pleasure to thank my thesis adviser, Professor E. N. Parker, for a number of stimulating discussions during the course of this work. I also benefited from conversations with Jacques Beckers, Arieh Königl, and Robert Rosner. This work was supported by the National Aeronautics and Space Administration under grant NGL 14-001-001.

APPENDIX

CONVECTIVE CONDITION IN POLYTROPIC ATMOSPHERES

The usual convective condition in a stratified gaseous atmosphere is

$$\frac{dT}{dz} = \left(1 - \frac{1}{\gamma}\right) \frac{T}{p} \frac{dp}{dz},$$

where γ is the adiabatic index (see, for example, Schwarzschild 1965, p. 50). Using equation (58), we obtain

$$\alpha' \frac{dT}{T} = \frac{dp}{p}. \tag{A1}$$

Equations (44) and (46) indicate that

$$p \propto T^{\alpha}$$

in a polytropic atmosphere, α being the polytropic index. Hence, from equation (A1),

$$\alpha' = \alpha.$$

This is our equation (60) and gives the convective condition in a polytropic atmosphere.

REFERENCES

Abdussamatov, H. I. 1976, *Solar Phys.*, **48**, 117.
Adjabshirzadeh, A., and Koutchmy, S. 1980, *Astr. Ap.*, **89**, 88.
———. 1982, *Solar Phys.*, **75**, 71.
Antia, H. M., and Chitre, S. M. 1979, *Solar Phys.*, **63**, 67.
Antia, H. M., Chitre, S. M., and Gokhale, M. H. 1978, *Solar Phys.*, **60**, 31.
Beckers, J. M., and Schneeberger, T. J. 1977, *Ap. J.*, **215**, 356.
Beckers, J. M., and Schröter, E. H. 1968, *Solar Phys.*, **4**, 303.
———. 1969, *Solar Phys.*, **10**, 384.
Biermann, L. 1941, *Vierteljahrsschr. Astr. Ges.*, **76**, 194.
Bonet, J. A., Ponz, J. D., and Vasquez, M. 1982, *Solar Phys.*, **77**, 69.
Bray, R. J., and Loughhead, R. E. 1964, *Sunspots* (New York: Wiley).
Bumba, V., Hejna, L., and Suda, J. 1975, *Bull. Astr. Inst. Czechoslovakia*, **26**, 315.
Bumba, V., and Suda, J. 1980, *Bull. Astr. Inst. Czechoslovakia*, **31**, 101.
Chandrasekhar S. 1952, *Phil. Mag.*, Ser. 7, **43**, 501.
———. 1961, *Hydrodynamic and Hydromagnetic Stability* (Oxford: Clarendon Press).
Chapman, G. A. 1974, *Ap. J.*, **191**, 255.
Chevalier, S. 1916, *Ann. Obs. Astr. Zô-sè*, **9**, B1.
Danielson, R. E. 1964, *Ap. J.*, **139**, 45.
Defouw, R. J. 1976, *Ap. J.*, **209**, 266.
Frazier, E. N., and Stenflo, J. O. 1972, *Solar Phys.*, **27**, 330.
Gokhale, M. H., and Zwaan, C. 1972, *Solar Phys.*, **26**, 52.
Gough, D. O., and Taylor, R. J. 1966, *M.N.R.A.S.*, **133**, 85.
Hasan, S. S. 1984, *Ap. J.*, **285**, 851.
Hejna, L. 1977, *Bull Astr. Inst. Czechoslovakia*, **28**, 126.
Howard, R., and Stenflo, J. O. 1972, *Solar Phys.*, **22**, 402.
Kneer, F. 1973, *Solar Phys.*, **28**, 361.
Knobloch, E., and Weiss, N. O. 1984, *M.N.R.A.S.*, **207**, 203.
Koutchmy, S., and Adjabshirzadeh, A. 1981, *Astr. Ap.*, **99**, 111.
Krat, V. A., Karpinsky, V. N., and Pravdjuk, L. M. 1972, *Solar Phys.*, **26**, 305.
Lawrence, J. K. 1983, *Solar Phys.*, **87**, 1.
Livingston, W., and Harvey, J. 1969, *Solar Phys.*, **10**, 294.
Loughhead, R. E., Bray, R. J., and Tappere, E. J. 1979, *Astr. Ap.*, **79**, 128.
Makita, M., 1963, *Pub. Astr. Soc. Japan.*, **15**, 145.
Meyer, F., Schmidt, H. U., Weiss, N. O., and Wilson, P. R. 1974, *M.N.R.A.S.*, **169**, 35.
Mogilevsky, E. J., Demika, L. B., Ioshpa, B. A., and Obridko, V. N. 1968, in *IAU Symposium 35, Structure and Development of Solar Active Regions*, ed. K. O. Kiepenheuer (Dordrecht: Reidel), p. 215.
Moor, R. L. 1981, in *The Physics of Sunspots*, ed. L. E. Cram and J. H. Thomas (Sunspot: Sacramento Peak Observatory), p. 259.
Moore, R., and Rabin, D. 1985, *Ann. Rev. Astr. Ap.*, **23**, 239.
Muller, R. 1973*a*, *Solar Phys.*, **29**, 55.
———. 1973*b*, *Solar Phys.*, **32**, 409.
———. 1976, *Solar Phys.*, **48**, 101.
———. 1981, in *The Physics of Sunspots*, ed. L. E. Cram and J. H. Thomas (Sunspot: Sacramento Peak Observatory), p. 340.
Nye, A. H., and Thomas, J. H. 1974, *Solar Phys.*, **38**, 399.
Obridko, V. N. 1968*a*, *Bull. Astr. Inst. Czechoslovakia*, **19**, 183.
———. 1968*b*, *Bull. Astr. Inst. Czechoslovakia*, **19**, 186.
———. 1975, *Soviet Astr.*, **18**, 758.
Parker, E. N. 1974*a*, *Solar Phys.*, **36**, 249.
———. 1974*b* *Solar Phys.*, **37**, 127.
———. 1979*a*, *Cosmical Magnetic Fields* (Oxford: Clarendon Press).
———. 1979*b*, *Ap. J.*, **230**, 905.
———. 1979*c*, *Ap. J.*, **234**, 333.
Priest, E. R. 1982, *Solar Magnetohydrodynamics* (Dordrecht: Reidel).
Proctor, M. R. E., and Weiss, N. O. 1982, *Rept. Progr. Phys.*, **45**, 1317.
Roberts, B., and Webb, A. R. 1978, *Solar Phys.*, **56**, 5.
Schwarzschild, M. 1965, *Structure and Evolution of the Stars* (New York: Dover).
Severny, A. B. 1965, *Soviet Astr.—AJ*, **9**, 171.
Sheeley, N. R. 1967, *Solar Phys.*, **1**, 171.
Soltau, D. 1982, *Astr. Ap.*, **107**, 211.
Spruit, H. C. 1974, *Solar Phys.*, **34**, 277.
———. 1977, *Solar Phys.*, **55**, 3.
———. 1979, *Solar Phys.*, **61**, 363.

Spruit, H. C., and Zweibel, E. 1979, *Solar Phys.*, **62**, 15.
Stenflo, J. O. 1973, *Solar Phys.*, **32**, 41.
Thomas, J. H. 1981, in *The Physics of Sunspots*, ed. L. E. Cram and J. H. Thomas (Sunspot: Sacramento Peak Observatory), p. 345.
Thomas, J. H., and Scheuer, M. A. 1982, *Solar Phys.*, **79**, 19.
Thomson, W. B. 1951, *Phil. Mag.*, Ser. 7, **42**, 1417.
Tönjes, K., and Wöhl, H. 1982, *Solar Phys.*, **75**, 63.
Webb, A. R., and Roberts, B. 1978, *Solar Phys.*, **59**, 249.
Wilson, P. R. 1969, *Solar Phys.* **10**, 404.
———. 1972, *Solar Phys.*, **22**, 434.
Zwaan, C. 1968, *Ann. Rev. Astr. Ap.*, **6**, 135.
Zwaan, C., and Buurman, J. 1971, in *IAU Symposium 43, Solar Magnetic Fields*, ed. R. Howard (Dordrecht: Reidel), p. 220.

ARNAB RAI CHOUDHURI: High Altitude Observatory, National Center for Atmospheric Research, PO Box 3000, Boulder, CO 80307